AIP ADVANCES **4**, 097122 (2014)

Solvothermal synthesis of NiAl double hydroxide microspheres on a nickel foam-graphene as an electrode material for pseudo-capacitors

Damilola Momodu,[1] Abdulhakeem Bello,[1] Julien Dangbegnon,[1] Farshad Barzeger,[1] Fatimeh Taghizadeh,[1] Mopeli Fabiane,[1] A. T. Charlie Johnson,[2] and Ncholu Manyala[1,a]

[1]*Department of Physics, Institute of Applied Materials, SARChI Chair in Carbon Technology and Materials, University of Pretoria, Pretoria 0028, South Africa.*

[2]*Department of Physics and Astronomy, University of Pennsylvania, Philadelphia, Pennsylvania 19104, USA*

(Received 12 August 2014; accepted 8 September 2014; published online 17 September 2014)

In this paper, we demonstrate excellent pseudo-capacitance behavior of nickel-aluminum double hydroxide microspheres (NiAl DHM) synthesized by a facile solvothermal technique using tertbutanol as a structure-directing agent on nickel foam-graphene (NF-G) current collector as compared to use of nickel foam current collector alone. The structure and surface morphology were studied by X-ray diffraction analysis, Raman spectroscopy and scanning and transmission electron microscopies respectively. NF-G current collector was fabricated by chemical vapor deposition followed by an ex situ coating method of NiAl DHM active material which forms a composite electrode. The pseudocapacitive performance of the composite electrode was investigated by cyclic voltammetry, constant charge–discharge and electrochemical impedance spectroscopy measurements. The composite electrode with the NF-G current collector exhibits an enhanced electrochemical performance due to the presence of the conductive graphene layer on the nickel foam and gives a specific capacitance of 1252 F g^{-1} at a current density of 1 A g^{-1} and a capacitive retention of about 97% after 1000 charge–discharge cycles. This shows that these composites are promising electrode materials for energy storage devices. [http://dx.doi.org/10.1063/1.4896125]

I. INTRODUCTION

The rapid development in the energy sector and the global economy has given rise to an urgent need for new technologies associated with the production and storage of energy. The uncontrollable depletion of fossil fuels and petroleum, with an increasing deterioration of the environment, has further increased the interest in energy research. In numerous applications, the most common, effective and practical technologies for electrochemical energy storage are batteries and electrochemical supercapacitors (ECs).[1,2]

ECs, (which comprises of electric double layer capacitors (EDLCs) or pseudocapacitors, based on their charge storage mechanism) have high power density, long cycle life and low maintenance cost as compared with batteries and conventional dielectric capacitors. Such outstanding characteristics are interesting for a wide range of applications such as mobile electronic devices, power/memory back-up systems, emergency units and hybrid vehicles.[1–4] However, the energy density of ECs is still an order of magnitude lower than that of the hybrid lithium-ion batteries in use today.[5] This limits their use in high-longevity and high-energy density applications. Thus there is an urgent need

[a]Author to whom correspondence should be addressed. Electronic mail: ncholu.manyala@up.ac.za

for the further development of high-performance electro-active and hybrid supercapacitive materials since the energy density is proportional to the specific capacitance of ECs.

Transition-metal oxides (MnO_2,[5,6] Fe_3O_4,[7] NiO)[8,9] and hydroxides ($Co(OH)_2$,[10,11] $Ni(OH)_2$)[12,13] are promising electrode materials for supercapacitor applications. The numerous studies carried out have yielded excellent supercapacitance values with some showing commendable energy densities which depict a promising future for these materials. Among these, a report by Bello *et al.*[5] illustrated using a simple hydrothermal reduction approach to anchor needle-like manganese oxide onto the surface of graphene foam (GF) grown by the atmospheric pressure chemical vapor deposition (AP-CVD) technique. The symmetric supercapacitor consisting of GF/MnO_2 composite exhibited a high capacitance value of 240 F g^{-1} at a current density of 0.1 A g^{-1} composite supercapacitors. A maximum energy density of 8.3 Whkg^{-1} was obtained, with a power density of 20 kWkg^{-1} and no capacitance loss after 1000 cycles. From the study, GF was seen as an excellent support for pseudo-capacitive oxide and hydroxide materials due to the combination of both electric double layer and pseudocapacitance properties.[5] Li *et al.*[13] also studied amorphous $Ni(OH)_2$ nanospheres fabricated by a simple green electrochemistry technique using cleaned graphite electrodes and obtained a specific capacitance of 153 F g^{-1} at a scan rate of 5 mV s^{-1}, with corresponding energy and power densities of 35.7Wh kg^{-1} and 490 W kg^{-1} respectively in an asymmetrical pseudocapacitor with activated carbon (AC) as the negative electrode.

Recently, layered-double hydroxides (LDHs) and double hydroxide microspheres (DHMs) containing transition metals have also been investigated as active electrode materials for supercapacitors.[14–20] A general chemical formula of $[M^{2+}{}_{1-x}M^{3+}{}_{x}(OH)_2]^{x+}[A^{n-}{}_{x/n}]^{x-}.mH_2O$ is used to synthesis LDH and DHM materials where M^{2+} and M^{3+} are divalent and trivalent cations respectively; A^n is a charge-balancing n-valent anion which usually comes from the precursor salts used in the preparation of the active material; and $x = M^{3+}/(M^{2+}+M^{3+})$. LDHs have an attractive redox property and since most of their growth techniques are environmentally friendly, they have great potential application as electrode materials for pseudocapacitors.[15,16] In addition, their tunable composition and flexible ion-exchangeability also add to the wide range of applications, including sensors, catalysts, drug delivery and matrix materials in hybrid composites, etc.[17,21–23] In particular, the growing interest in their use in electrochemical capacitors is generally due to the active chemical sites present for both electric double layer capacitors and pseudocapacitors.[24] However, they are characterized by relatively low electron transfer and mass diffusion which inhibits the rate of charge–discharge properties and affects their overall electrochemical performance. Hence a composite material that will provide a suitable support for the active material while improving the surface interaction between the current collector and the LDH material is ideal.

Graphene-based supercapacitor electrodes have attracted much attention due to their unique properties such as high electrical conductivity, high surface area and robust mechanical properties.[25–28] In recent studies, Khamlich *et al.*[26] used an in situ aqueous chemical growth technique of simonkolleite ($Zn_5(OH)_8Cl_2 \cdot H_2O$) onto nickel foam-graphene (NF-G) to form a NF-G/simonkolleite composite that acted as an active electrode material with a specific capacitance of 350 F g^{-1} at 0.7 A g^{-1}. Another report by Dong *et al.*[27] adopted an innovative strategy of in situ growth of cobalt oxide (Co_3O_4) nanowires on 3D graphene foam grown by CVD. The graphene/Co_3O_4 composite was used as a monolithic free-standing supercapacitor electrode and exhibited a high specific capacitance of ~1100 F g^{-1} at a current density of 10 A g^{-1} with excellent cycling stability after 1000 cycles. Despite these achievements, if the desire to store energy efficiently is to be met, the need to synthesize materials with higher specific capacitance, combined with an excellent rate performance and even better long-lasting stability, is still crucial. In this regard, most recent studies are therefore inclined towards achieving well-defined micro/nanostructures with excellent surface properties, better electrochemical performance, higher electrical conductivity and adequate pore size distribution in order to enhance interface reactions and enhance the mass/electron transfer of the electroactive species during faradaic redox reactions.[17,29] Song *et al.*[29] used a solvothermal technique in which the ratio of ethanol/water was varied to obtain different structures of NiAl LDHs. The sample prepared with 100% ethanol had a specific surface area of about 300 m^2 g^{-1}. According to their report, 3D flowerlike porous structures assembled by 2D anisotropic LDH nanosheets were obtained using an ethanol solvent alone during the solvothermal growth. Tao *et al.*[30] also

used a tertbutanol-water (TBA-H_2O) mixture as a structure-directing agent to tune the morphology and nanostructure of nickel/cobalt double hydroxide microspheres (Ni-Co DHM). By varying the TBA:H_2O ratio, a unique microspherical architecture of synthesized Ni-Co DHMs was obtained with a 9:1 (TBA:H_2O) ratio with high supercapacitance and excellent capacitance retention at a cycling current density of 10 A g^{-1}.

In this study, TBA was also adopted as a structure-directing agent to fabricate nickel-aluminum double hydroxide microspheres (NiAl DHMs). These unique architectures could potentially improve the faradaic redox reactions and mass transfer. Thus, the pseudocapacitive performance of these microspheres was measured. The active material was coated on a nickel foam-graphene (NF-G) current collector prepared by AP-CVD technique and the electrochemical characterization was performed in a three-electrode configuration. This active electrode exhibited an improved capacitance on NF-G compared with when nickel foam (NF) alone was used as the current collector. Good cyclic retention of 97% after 1000 cycles was also observed for the NiAl DHMs on NF-G current collector. These results demonstrate that the NiAl DHMs are possible material for use in energy storage/conversion devices.

II. EXPERIMENTAL

A. Material Synthesis

1. Synthesis of NiAl DHMs

Urea (Merck, purity $\geq$ 98%), Ni $(NO_3)_2.6H_2O$ and Al $(NO_3)_3.9H_2O$ (Sigma-Aldrich, purity $>$ 99.99%) were used as received without any further purification. The NiAl DHMs were synthesized by a facile and environmentally friendly solvothermal technique with a TBA-H_2O mixture used as solvent, in a ratio of 9:1. In a typical synthesis procedure, 1.8 mmol of $Ni^{2+}$and 0.6 mmol of Al^{3+} salts were added to a TBA-H_2O solution containing 0.5 g of urea. The solution was subjected to ultrasonic treatment for 20 minutes to ensure complete dispersion and dissolution of the salts, after which it was poured into a 200 ml Teflon-lined hydrothermal autoclave system. The vessel was transferred to an electric oven where it was kept at 120 °C for 19 h. After this reaction time, the vessel was allowed to cool down naturally to room temperature. Finally, the solution was filtered and the product was washed several times with deionized water and subsequently left to dry in an oven at 60 °C for 12 h.

2. Synthesis of nickel foam-graphene (NF-G) current collector

The nickel foam-graphene current collector was prepared by an AP-CVD technique. Briefly, a known mass of compressed circular nickel foam template (Alantum, Munich, Germany), with an areal density of 420 g m^{-2} and a diameter of 16 mm, was placed in a quartz tube for the CVD growth of graphene. The nickel foam was first annealed at 800 °C in the presence of Ar and H_2 gas for 60 minutes, prior to the introduction of the carbon source (CH_4 gas) at 1000 °C. The flow rates of the gases Ar:H_2:CH_4 were 300:9:15 SCCM respectively. After 60 minutes of deposition, the samples were rapidly cooled by manually pushing the quartz tube to a lower temperature region.

3. Electrode preparation

The working electrode was fabricated using the method described in the earlier report by Bello *et al.*[5] The procedure involved mixing 80 wt. % of the active material (NiAl DHM powder) with 10 wt. % of carbon black (CB) and 10 wt. % polyvinylidene difluoride (PVdF) binder in an agate mortar. A paste made from this mixture is achieved by adding a few drops of 1-methyl-2-pyrrolidinone (NMP) to the mixture. The paste was coated on the NF-G and also on the NF current collectors respectively, for comparison. The coated samples were dried in an oven at 60 °C for 12 h to ensure complete evaporation of the NMP.

B. Material Characterization

Scanning electron microscopy (SEM) and transmission electron microscopy (TEM) analyses were carried out to reveal the morphology and microstructure of the sample using a Zeiss Ultra Plus 55 field emission scanning electron microscope (FE-SEM) operated at an accelerating voltage of 2.0 kV, and a JEOL JEM-2100F microscope operated at 200 kV respectively. Typically, SEM and TEM samples were prepared by dispersing them in ethanol and dropping them on glass substrates and lacey carbon-coated copper grids respectively for analysis. The sample was also characterized using powder X-ray diffraction (XRD). An XPERT-PRO diffractometer (PANalytical BV, Netherlands) with theta/theta geometry, operating a cobalt tube at 35 kV and 50 mA, was used. The XRD patterns of all specimens were recorded in the 10.0° – 80.0° 2θ range with a counting time of 15.240 seconds per step. Qualitative phase analysis of the sample was conducted using the X'pert Highscore search match software. Fourier transform infrared (FT-IR) spectra of the NiAl DHMs were recorded using a Bruker Vertex 77v FT-IR spectrometer, while the Raman spectra were obtained using a Jobin–Yvon Horiba TX 6400 micro-Raman spectrometer equipped with a triple monochromator system to eliminate contributions from Rayleigh scattering. The samples were excited using the 514 nm wavelength of an argon laser. The laser was focused on the sample using a 509 objective with 100x magnification and the acquisition time of each spectrum was 60 s. Surface area measurements were obtained using the Brunauer-Emmett-Teller (BET) method with N_2 gas. Pore size and pore volume were obtained using Barrett-Joyner-Halenda (BJH) method from the desorption branch of the isotherm.

C. Electrochemical Measurement

The capacitive properties were investigated using a Bio-Logic SP300 workstation (Knoxville TN 37930, USA) in a three-electrode configuration controlled by the EC-Lab® V10.37 software. The electrochemical test was performed also in a three-electrode configuration with the as-prepared NiAl DHM serving as the working electrode in 6 M potassium hydroxide (KOH) electrolyte, glassy carbon plate as the counter electrode and Ag/AgCl (3 M KCl) as the reference electrode.

The cyclic voltammetry tests were carried out in the potential range of 0 to 0.5 V (vs. Ag/AgCl) at different scan rates ranging from 5 to 100 mV s^{-1}. The galvanostatic charge–discharge measurements were also carried out at different current densities from 1 to 5 A g^{-1} and the electrochemical impedance spectroscopy (EIS) measurements were performed in the frequency range of 100 kHz–10 mHz.

III. RESULTS AND DISCUSSION

A. Morphology and Structure

Fig. 1 shows the morphology of the NiAl DHMs from microscopy analysis. Figs. 1(a) and 1(b) show nanoflakes interlaced with each other to form spherical microstructures with an average diameter of 1 μm at different magnifications. Thin flake-like structures are observed from the TEM micrographs, as shown in Figs. 1(c) and 1(d) also at different magnifications. These structures are ideal for electrochemical applications that involve interface reactions. Similar structures were obtained in earlier work by Tao *et al.*[30] in which Ni-Co hydroxide microspheres were hydrothermally synthesized in the same TBA:H_2O ratio of 9:1. The mechanism of the formation was explained to be due to the viscous nature and the spatial structure of the TBA solvent compared with other similar small molecule solvents.

In a particular ratio of TBA:H_2O, the TBA molecules self-assemble to form a nanoemulsion with the surface necessary for the growth of nanoflakes during the solvothermal process.[30,31] To describe the possible formation of the NiAl DHMs, which are spherical layered double hydroxides (LDHs), we refer to the Ostwald ripening mechanism which involves the nucleation and growth of NiAl LDH crystals.[29] In other words, in the presence of a mixture of Ni^{2+} and Al^{3+} salts, the continuous supply

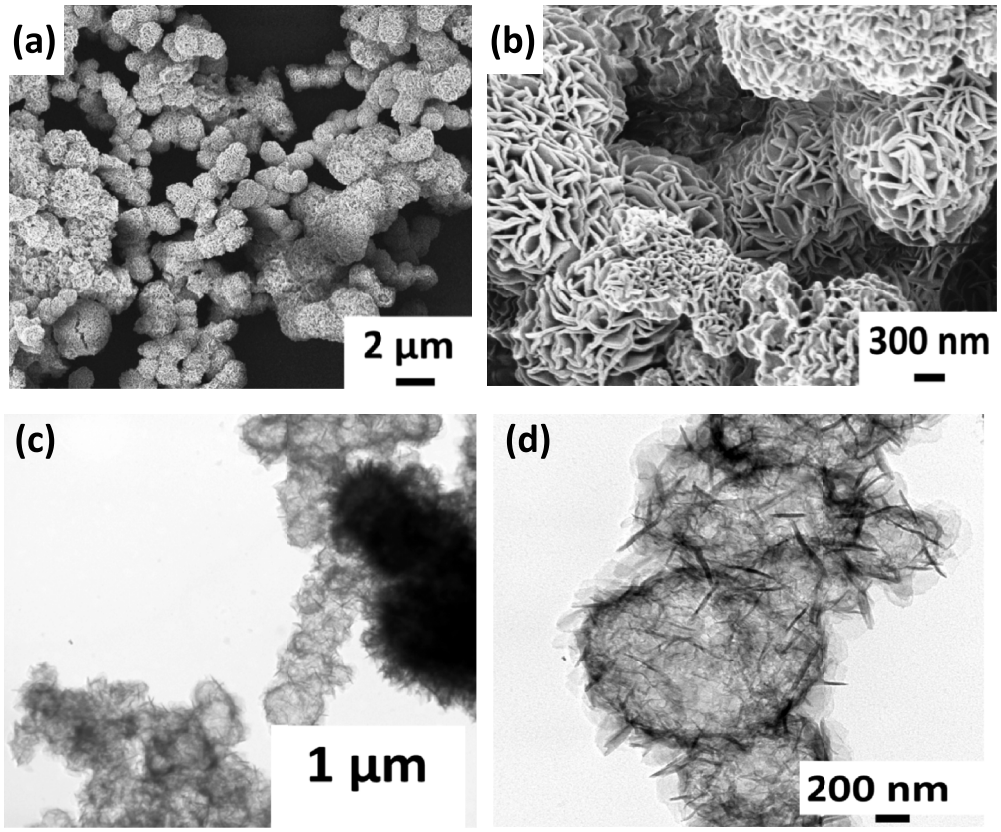

FIG. 1. (a, b) SEM micrograph of NiAl DHM; (c,d) TEM images of NiAl DHM at different magnifications.

of carbonate (CO_2^-) and hydroxide (OH^-) at a controlled rate from urea decomposition leads to the formation of the founding double hydroxide nanoparticles.[14]

The whole evolution/growth process could be likened to the three-stage process reported in previous studies[32] which involves a fast nucleation of amorphous primary particles, followed by crystal growth and final self-assembly. Over the course of the reaction, the concentration of the reactants in the reaction medium is decreased and a chemical equilibrium between the solid–liquid interfaces is established.

Meanwhile, the smaller interior crystallites are still in a non-equilibrium state. In this process, the exterior crystallites will serve as starting points to attract the smaller metastable crystallites. Subsequently, double hydroxide nanosheets gradually grow into their final form.[33] Many forces contribute to this unique structure, including electrostatic forces, crystal–face interaction, hydrogen bonds and van der Waals forces.[34]

The SEM micrographs in Fig. 2(a) to 2(d) display the morphology of the NF and NF-G current collectors at different magnifications. Fig. 2(b) shows the grain boundaries of nickel at higher magnifications, while the wrinkled nature of continuous few-layer graphene covering the nickel surface is shown in Fig. 2(d). The wrinkles are formed during the rapid cooling process that is necessary for the out-diffusion of carbon atoms onto the NF surface to form graphene layers. Due to the difference in the thermal expansion coefficients of the NF substrate and the grown graphene layer, these wrinkles appear as a result of the release of strain occurring from this mismatch.[35] The SEM micrographs in Figs 2(e) and 2(f) show the nature of the coating of the NF-G current collector with the NiAl DMH active material mixed with carbon black and PVdF binder. The active material is seen to fill in the pores of the NF-G current collector material. The spherical nature of the active material is seen to be retained in the higher magnification image of Fig. 2(f), although other materials have been added to form the paste coated onto the NF-G.

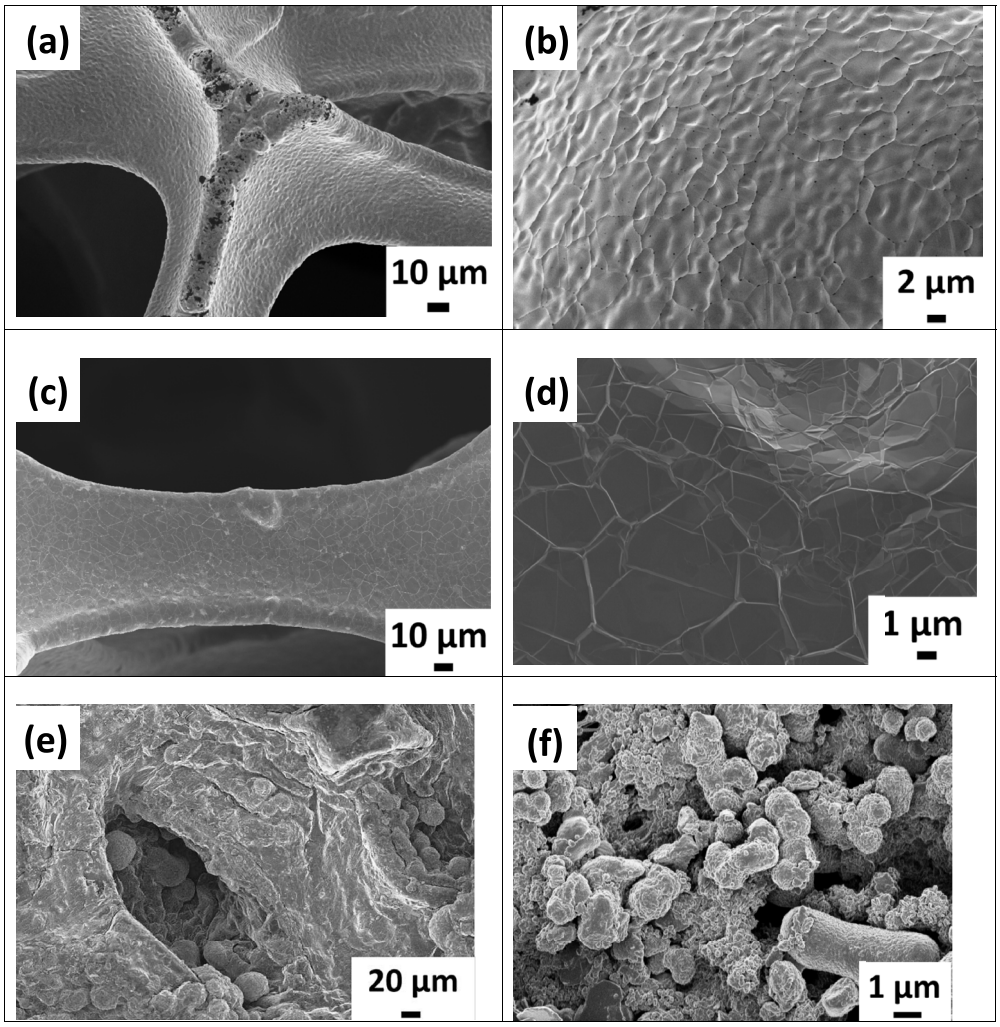

FIG. 2. SEM micrograph of (a,b) NF; (c,d) NF-G grown by CVD at different magnifications; (e, f) NiAl DHM paste coated on NF-G at different magnifications.

Figs 3(a) and 3(b) show the XRD patterns of the synthesized NiAl DHM powder and the composite electrode material, with typical diffraction peaks indexed to a hydrotalcite-like structure for LDH [Joint Committee on Powder Diffraction Standards (JCPDS) 15-0087/01-089-1777)], Ni and graphene respectively. The NiAl DHM peaks are also similar to those reported in earlier studies[14] in which characteristic reflection patterns of the LDH structure were studied, showing strong peaks with their relatively high crystallinity. However, these peaks exhibit a shift due to the nature of the X-ray source (cobalt) used in the analysis of the samples. For example, the reflection from the (003) plane with a strong diffraction peak usually ascribed to the 2θ angle of $\sim 11.30^{\circ}$[14] is now observed at 13.1°. Likewise, similar peak shifts exist for other planes, such as the (006), (015), (018) and (110) planes, which show diffraction peaks at 2θ values of 26.7°, 40.7°, 47.5° and 72.7° respectively. The shifts are due to the difference in wavelength of the incoming X-rays which are dependent on the X-ray source, according to the Bragg equation: $n\lambda = 2\mathrm{d}\sin\theta$. In general, X-rays from a cobalt source ($\lambda = 1.79$ Å) with longer wavelengths result in greater 2θ positions compared with those from a copper source ($\lambda = 1.54$ Å). The former usually allows the observation of low-angle peaks that are not observable using the shorter wavelength X-rays and provides better peak separation.[36]

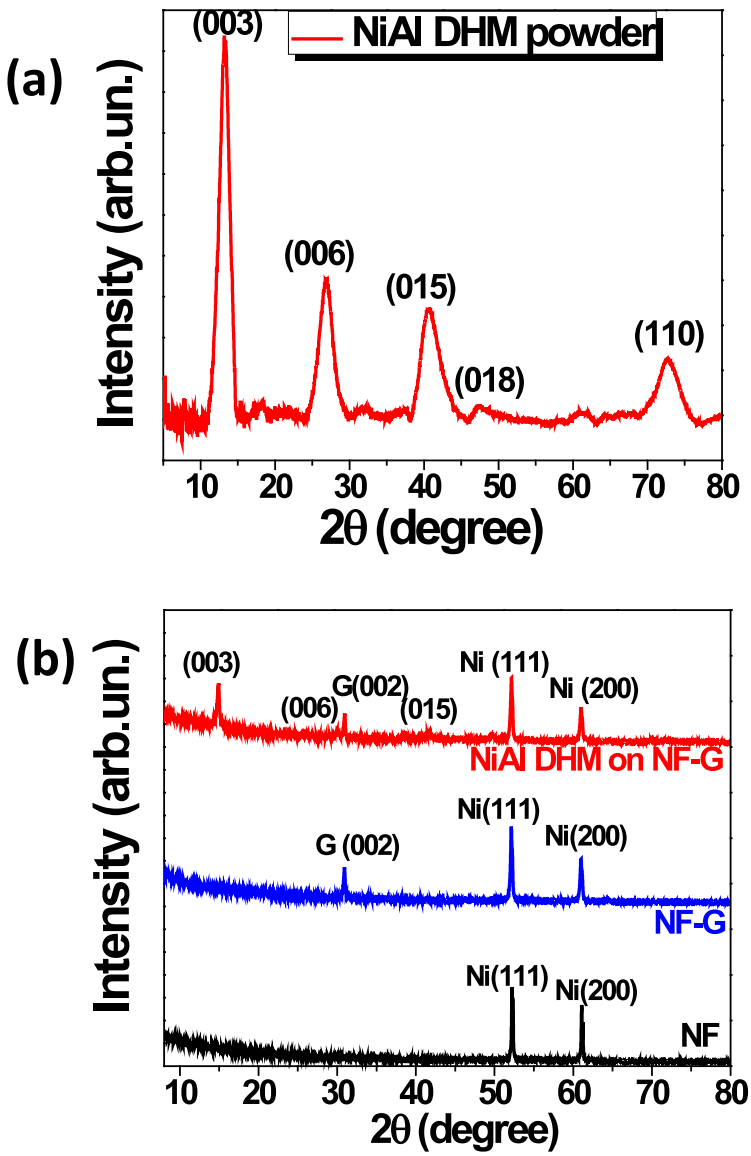

FIG. 3. (a) XRD patterns of NiAl DHM powder and (b) XRD pattern of NF, GF, NF-G and NiAl DHM on NF-G.

These observed peaks indicate that the sample analyzed is a layered structure belonging to a hydroxide layered system and to NiAl DHM in particular. The *d*-spacing of the (003) and (006) planes are dependent on the charge and the size of the charge-balancing interlayer anion. When CO_3^{2-} is the interlayer anion, the *d*-spacing values are approximately 0.78 nm and 0.39 nm for the (003) and (006) planes respectively.[37,38] From the position of the (003) and (006) reflections, *d*-spacing values of 0.78 nm and 0.39 nm were obtained when calculated with the XRD data thus confirming the CO_3^{2-} intercalation. The CO_3^{2-} ions could arise from the deionized water and the decomposition of urea. The gallery height, which was calculated by subtracting the thickness of the brucite-like layer (0.477 nm)[39] from the thickness of the unit layer ($d_{(0\,0\,3)}$ basal spacing), is 3.07 nm. This value is lower than the corresponding free anion diameter (D = 0.37 nm), which implies strong interaction of the anion with the brucite-like layer.[40] The XRD patterns for the coated material on the different current collectors are also shown in Fig. 3(b) with their characteristic peaks. The XRD pattern for NF consists of two very strong peaks recorded at 52.1° and 60.9°, which could be assigned to the (1 1 1), (2 0 0) phase of nickel. The diffraction peak at $2\theta = 31°$ corresponds to the

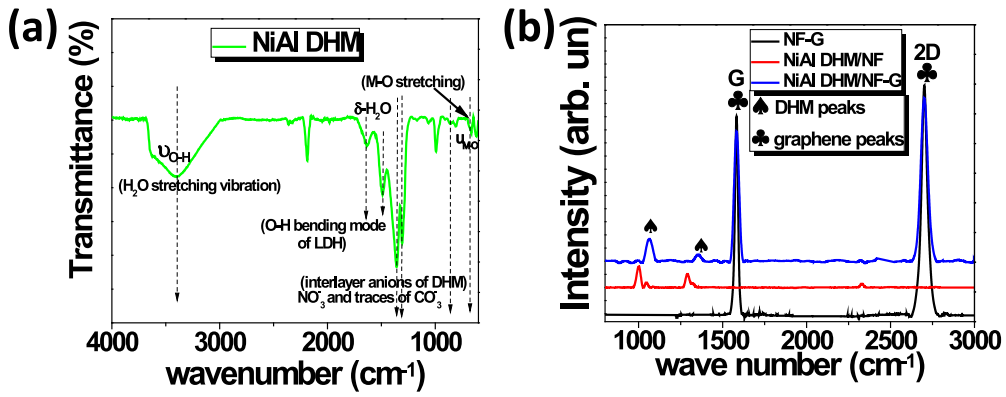

FIG. 4. (a) FT-IR spectra for NiAl DHM and (b) Raman spectra for NF-G, NiAl DHM on NF and NF-G.

(002) reflection of hexagonal graphitic carbon, which is an indication of the presence of graphene (G).[8,41] For the XRD pattern of the active material on the NF-G current collector, all characteristic reflections of NiAl DHMs, NF and G are observed and indexed as shown.

Figs. 4(a) and 4(b) show the FT-IR and Raman spectroscopic images of the NiAl DHM on the NF and NF-G templates respectively. These measurements were performed to determine the nature of the material from the different vibration modes arising from the excitation of the samples. Furthermore, this technique can give good insights into the type of the interlayer anion. The infrared spectrum of the NiAl DHM powder is shown in Fig. 4(a) within a range from 600 to 4000 cm^{-1}. A broad absorption band centered at about 3408 cm^{-1} corresponds to the O-H stretching vibrations of the interlayer water molecules and the hydrogen-bonded OH-groups of the hydrotalcite layers accompanied by bending at 1643 cm^{-1}.[17,42] The peaks at 1300 and 1363 cm^{-1} originate from vibrations of the interlayer CO_3^{2-} anions.[17] This is in good agreement with the XRD results which show evidence of the presence of CO_3^{2-} charge-balancing interlayer anions. The remaining bands below 800 cm^{-1} are attributed to metal-oxygen (M-O)/metal-hydroxyl (M-OH) stretching and bending modes (with M corresponding to Ni and Al).[42–44]

Fig. 4(b) shows the Raman spectra for NF-G, NiAl DHM on NF (NiAl-DHM/NF) and NF-G (NiAl-DHM/NF-G) respectively. The Raman spectrum in Fig. 4(b) for pure NF-G shows the characteristic G-band and 2D-bands associated with graphene vibrational modes. The G-band arises from the first-order scattering of the E_{1g} phonon for sp^2 carbon atoms in the wavenumber region of 1500 – 1600 cm^{-1}.[45] The 2D peak in graphene is due to two phonons with opposite momentum in the highest optical branch near the A_1 symmetry at K point.[46] The Raman spectra for NiAl DHM/NF and NiAl DHM/NF-G exhibit features that are typical of NiAl hydrotalcite structure. The peaks at 1049 cm^{-1} and 1331 cm^{-1} are typical Raman peaks related to NiAl LDH.[19]

The supercapacitive performance of the active electrode material is dependent on its ability to accommodate as much active electrochemical sites for charge storage during operation. The presence of suitable mesopores within the electrode material is also ideal to ensure the reduction of mass transfer of electrolyte during fast redox reactions and facilitates power delivery.[17]

The physical adsorption/desorption of N_2 at 77K results shown in Fig. 5 displays the surface area and pore size distribution for the prepared NiAl DHM powder sample. Fig. 5(a) shows a type IV isotherm with a H_3-type hysteresis loop ($P/P_o > 0.4$) which indicates the presence of mesopores in the active double hydroxide material[17,47] with a specific surface area (SSA) of 90.36 $m^2\ g^{-1}$. This value is comparable to or even larger than those reported in earlier studies for NiAl-double hydroxide materials published elsewhere.[17,29,48] Fig. 5(b) shows the corresponding pore size distribution with a major pore diameter ranging from 1.7 to 4 nm which shows the successful inclusion of both microporous and mesoporous sites. The micropores (diameter <2 nm) present serve as the ion traps for energy storage, while the mesopores are used as pathways for transport of ions necessary for power delivery.[2,49]

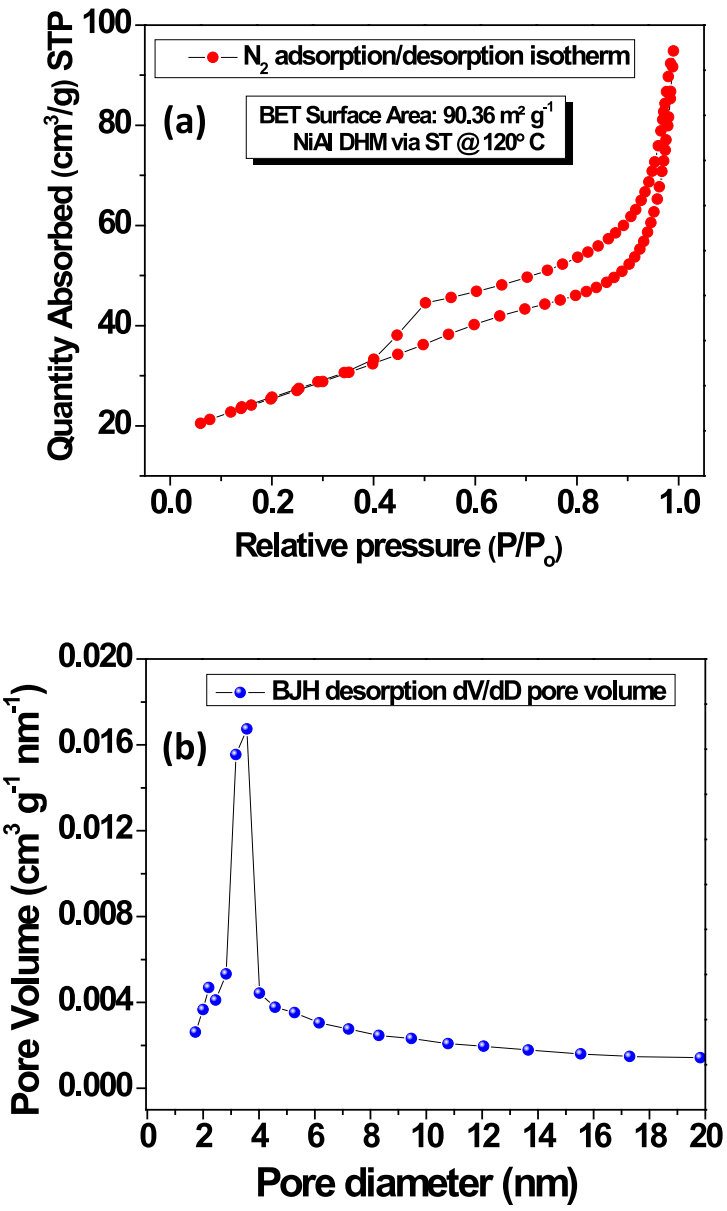

FIG. 5. (a) N_2-adsorption/desorption isotherms for NiAl DHMs; (b) the pore size distribution of the NiAl DHMs.

B. Electrochemical Performance

Cyclic voltammetry (CV) measurements are used to understand the macroscopic electrochemical surface reactions at the electrode material during operation. Fig. 6(a) shows the CV curves for a bare NF current collector, NF-G current collector, and NiAl DHMs coated onto NF (NiAl-DHM/NF) and NiAl DHM on NF-G (NiAl-DHM/NF-G) current collectors at a scan rate of 20 mV s^{-1}. The CV plots are characterized by symmetrical characteristic profiles that are well defined by cathodic (reduction reaction) and anodic (oxidation reaction) peaks.[30] This reveals that the electrode reaction corresponds to a quasi-reversible process, indicating that the measured capacitance in these materials is mainly based on the redox mechanism due to the pseudocapacitive behavior of the material.[50] It can be clearly seen that the integral area of the CV graph of NiAl DHM/NF-G curve is the largest among the three electrode materials presented, implying that it possesses the highest specific capacitance. This improvement in pseudocapacitance could be due to the contribution of

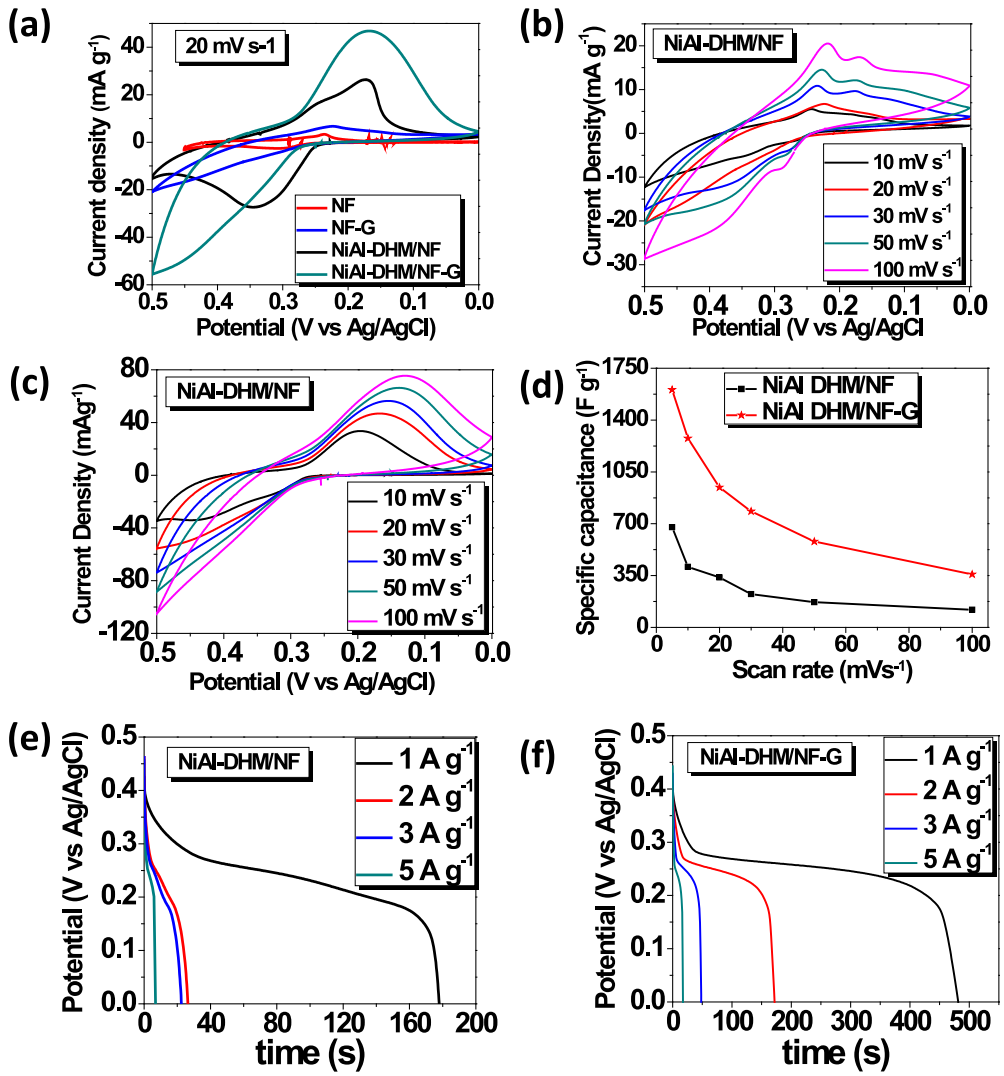

FIG. 6. (a) Cyclic voltammetry of NF, NF-G, NiAl DHM on NF and NF-G at a scan rate of 20 mV s^{-1}; cyclic voltammetry of NiAl DHM at different scan rates on (b) NF and (c) NF-G; (d) specific capacitance of NiAl DHM on NF and NF-G versus scan rates; (e) galvanostatic charge–discharge measured at different current densities for NiAl DHM on NF; (f) galvanostatic charge–discharge measured at different current densities for NiAl DHM on NF-G.

more electronegative species existing within the interlayer region of the LDH structure,[14,15] together with the high conductivity of the graphene on nickel foam.

Fig. 6(b) shows the CV plot for NiAl DHM/NF current collector at a scan rate ranging from 5 to 100 mV s^{-1} with redox peaks that undergo small shifts towards the negative potential with increasing scan rate. The first sets of peaks at 0.36 V and 0.23 V are related to the cathodic and anodic peaks of the NF current collector material at a scan rate of 30 mV s^{-1}. The second set of redox peaks shows symmetrical CV plots with well-defined redox peaks which occur at 0.28 V and 0.17 V respectively at the same scan rate. These peaks are related to the pseudocapacitive nature of NiAl DHM and the strong redox peaks correspond to the following redox reactions where Ni undergoes a transition between different oxidation states:[14]

$$Ni(OH)_2 + OH^- \leftrightarrow NiOOH + H_2O + e^- \quad (1)$$

Fig. 6(c) shows the CV plots of the NiAl DHM/NF-G with the cathodic and anodic peaks observed to occur at around 0.40 V and 0.15 V respectively at a scan rate of 30 mV s^{-1}. The peaks ascribed to

the NF current collector are not seen for NiAl DHM/NF-G; this could be assumed to be due to the complete coverage of NF by graphene thus confirming an effective coating of the NF surface with the graphene layer. The successful growth of a thin layer of graphene on the NF could be further confirmed from the current response value recorded from the CV plots when compared with those where NF current collector was used (Fig. 6(b)).

Using equation (2) below, the specific capacitance can be calculated from the CV:[17,51]

$$C_s\left(\frac{\mathrm{F}}{\mathrm{g}}\right) = \frac{\bar{A}}{m\Delta V\, \bar{f}} \tag{2}$$

where $\bar{A}$ is the integrated area under the curve for the cathodic current of the CV curve (in mA-V); m is the mass of the coated active material (in g); and f is the scan rate (in mV/s) used during the CV measurement. The specific capacitance calculated from the CV measurements is 409 F g^{-1} for NiAl DHM/NF; this increases to 1276 F g^{-1} when NF-G is used as current collector, both at a scan rate of 10 mV s^{-1}. The higher specific capacitance calculated for NiAl coated on NF-G may be due to the presence of the graphene layer deposited on the surface of the NF. This layer provides the higher conductivity required for fast ion transport at the electrolyte/electrode surface.

Fig. 6(d) shows the variation of the specific capacitance values with increasing scan rate; a decrease in specific capacitance is observed at a higher scan rate. Indeed, at a low scan rate, most of the electrode's active surface area is in good contact with the ions contained in the electrolyte, allowing complete interactions between them. However, at a higher scan rate, the effective interaction is greatly reduced, leading to lower observed specific capacitance values. Also at higher scan rates, the movement of ions is limited by the diffusion, and only outer active surfaces are used for charge storage, leading to lower specific capacitance values.[52]

The galvanostatic discharge plots for NiAl DHM/NF and NiAl DHM/NF-G are shown in Figs. 6(e) and 6(f) at current densities of 1, 2, 3 and 5 A g^{-1} respectively. An enhancement in the discharge time for the NiAl DHM/NF-G composite electrode at 1 A g^{-1} current density is observed in Fig. 6(f) as compared with that of NiAl DHM/NF (Fig. 6(e)). The specific capacitance was also calculated from the galvanostatic discharge curves using the formula:[14,17]

$$C_S\,(\mathrm{F/g}) = \frac{I T_{\mathrm{d}}}{m\Delta \mathrm{V}} \tag{3}$$

where I is a current (A), T_d is the discharge time (s), m is the mass of active material (g), and ΔV is the voltage range (V).

A specific capacitance of 1252 F g^{-1} is obtained for NiAl DHM/NF-G compared with a value of 354 F g^{-1} for NiAl DHM/NF at a current density of 1 A g^{-1}. This is an enhancement of 3.5 times for the NF-G current collector and is a great improvement over similar studies on NiAl DHM prepared by a solvothermal technique reported elsewhere.[29] We therefore propose that the improvement in supercapacitance value is a result of the addition of a graphene layer to form the NF-G current collector which provides an improved electron transfer rate and better structural support for the DHM material[26,30] and could also ensure the retention of the capacitance even after long cycling.

The stability of the electrode material of supercapacitors is also a very important characteristic for their application as energy storage devices. Figs 7(a) and 7(b) show the continuous cycling in galvanostatic charge–discharge and the associated capacitance retention of NiAl-DHM on both NF and NF-G current collectors, respectively, within a potential window of 0 – 0.5 V at a 30 A g^{-1} current density for 1000 cycles. The stability plot was characterized by little change in the specific capacitance obtained from repeated charging and discharging, which initially increased after 200 cycles before stabilizing at a higher number of cycles for both cases. This observation is unique to LDH-based materials and has also been previously reported in earlier studies.[17,42] It is suggested that this increase is as a result of the full exposure of some inner sites of the DHM material which were not exposed during the initial cycling stage, and due to the activation of NiAl LDH sites which contribute to an increase in capacitance after some initial cycling of the active electrode material.[17,42] The capacitive retention stabilizes to a value of 97.9% for NiAl DHM on NF-G and to a slightly lower value of 95.7% for NiAl DHM on NF after 700 cycles. This is also an improvement over

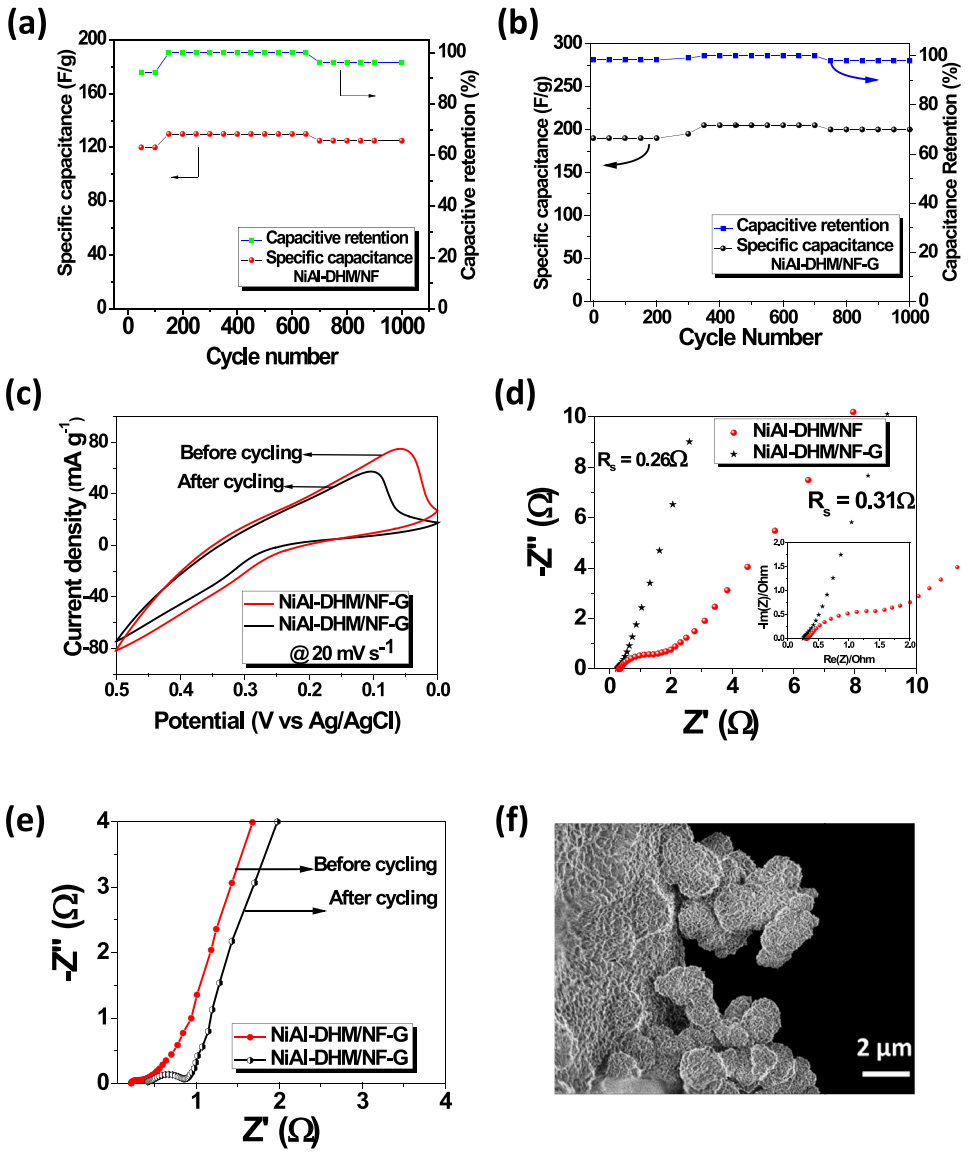

FIG. 7. Dependence of the cycling discharge specific capacitance and capacitive retention on the charge–discharge cycle numbers for NiAl DHM on (a) NF and (b) NF-G respectively at a current density of 30 A g^{-1}; (c) CV comparison of NiAl DHM on NF-G before and after cycling at a scan rate of 20 mV s^{-1}; (d) EIS of NiAl DHM on NF and NF-G current collector at a potential of 0.2 V; (e) EIS comparison of NiAl DHM on NF-G before and after cycling at a potential of 0.2 V; (f) SEM image for comparison of NiAl DHM on NF-G before and after cycling.

similar reports[29] for NiAl DHM prepared using a solvothermal technique where a solvent was used to direct the growth of the double layer hydroxides. Although a longer cycling time was adopted here as compared with that adopted by Song *et al.*,[29] an improvement from 95% to 97.5% was still observed for the capacitive retention. Since redox reactions also take place during the continuous cycling charge–discharge process, a comparison was made for the CV curves before and after cycling to further analyze the cyclic stability of the electrode material (i.e. NiAl DHM/NF-G in Fig. 7(c)). Similar CV curves were obtained (Fig. 7(c)) before and after the 1000th cycle; in other words, both CV curves appear with their usual redox peaks which confirm the stability of the NiAl DHM material. However, a slight reduction in the intensity and shift of the anodic peak positions towards

the positive potential is observed. This is caused by consumption of some of the active sites in the material which leads to some subsequent capacitance loss.[44]

Fig. 7(d) shows the Nyquist plots from the EIS test done at open circuit (E_{oc}) potential to further evaluate the electrochemical behavior for the NiAl DHM on NF and NF-G. The frequency range used for the measurement was from 10 mHz to 100 kHz. At high frequency, a partial semi-circular arc is formed which is attributed to the dispersion effect.[44] At low frequency, the impedance plot should, theoretically, be a vertical line parallel to the vertical -Im (Z) axis. This vertical line indicates a pure capacitive behavior of the DHMs and low diffusion resistance of ions within the structure of the material.[17] The electrode series resistance of the active material on both NF and NF-G was deduced from the intercept on the real Z-axis, while the charge transfer resistance (R_{ct}) was obtained based on the semi-circular arc radius.[44] The electrode series resistance value from the Nyquist plots improves from 0.31 Ω for NiAl DHM/NF to 0.26 Ω for NiAl DHM/NF-G due to the presence of a graphene layer on the NF current collector. From the inset to Fig. 7(d), the radius of the semi-circular arc is related to the resistance of the charge transfer process. This radius is also observed to be smaller for the NiAl DHM on NF-G when the partial semi-circular arc is extrapolated to a complete a semi-circle. These enhancements could be attributed to the better conductivity and favorable electron transfer rate when the NF-G current collector was used. A similar explanation for this occurrence was reported in an earlier study where GF grown by CVD was used as an electrode material.[27]

Fig. 7(e) shows the Nyquist plots for the NiAl DHM on NF-G before and after the last cycle. Both plots were characterized by semi-circular arcs with intercepts on the Z'–axis and an increase in the radius of the semi-circle after cycling is observed, which could be ascribed to a slight increase in the internal resistance. In principle, an increase in the internal resistance could be linked to the capacitance loss described earlier when referring to the decrease in intensity of the CV peaks. The morphological characterization of the electrode after cycling tests was done to conclude analysis on stability. The SEM image of the electrode showed the retention of the microspherical nature of the NiAl double hydroxides (Fig. 7(f)). Thus, these results show the suitable use of the electrode for full device supercapacitor applications.

IV. CONCLUSION

Using a facile solvothermal technique that is environmentally friendly, nickel-aluminum double hydroxide microspheres (NiAl DHMs) have been successfully prepared in a tertbutanol-water (TBA-H_2O) medium as a suitable electrode material for pseudocapacitor devices. This study demonstrated the unique morphology of the NiAl DHMs with relatively thin flakes grown on microspheres, as seen from the scanning and tunneling electron microscopy results. The addition of graphene to the surface of the pristine nickel foam (NF) current collector retains the spherical morphology, while greatly enhancing the electrochemical performance, electrical characteristics and stability of the DHMs. Overall, the simple strategy adopted to synthesize NiAl DHM structures and coat them on nickel foam graphene (NF-G) templates to fabricate electrodes with superior electrochemical properties makes NiAl DHMs a good and promising material for application in hybrid electrochemical capacitors.

ACKNOWLEDGMENTS

This work is based on research supported by the South African Research Chairs Initiative (SARChI) of the South African Department of Science and Technology (DST) and the National Research Foundation (NRF). Any opinion, findings and conclusions or recommendations expressed in this work are those of the authors and the NRF and DST do not accept any liability with regard thereto. A.T.C.J acknowledges support from the LRSM, through the U.S. National Science Foundation MRSEC, Grant No. DMR-1120901. D M acknowledges the financial support from the University of Pretoria and the NRF Doctorate Innovation Fund for his study. The authors will also like to acknowledge the invaluable discussions and inputs from Prof. Yury Gogotsi.

[1] B. Conway, J. Electrochem. Soc. **138**, 1539 (1991).
[2] C. Liu, F. Li, L.-P. Ma, and H.-M. Cheng, Adv. Mater. **22**, E28 (2010).
[3] A. Burke, J. Power Sources **91**, 37 (2000).
[4] P. Simon and Y. Gogotsi, Nat. Mater. **7**, 845 (2008).
[5] A. Bello, O. O. Fashedemi, J. N. Lekitima, M. Fabiane, D. Dodoo-Arhin, K. I. Ozoemena, Y. Gogotsi, A. T. Charlie Johnson, and N. Manyala, AIP Adv. **3**, 082118 (2013).
[6] G. Yu, L. Hu, M. Vosgueritchian, H. Wang, X. Xie, J. R. McDonough, X. Cui, Y. Cui, and Z. Bao, Nano Lett. **11**, 2905 (2011).
[7] D. Liu, X. Wang, X. Wang, W. Tian, J. Liu, C. Zhi, D. He, Y. Bando, and D. Golberg, J. Mater. Chem. A **1**, 1952 (2013).
[8] A. Bello, K. Makgopa, M. Fabiane, D. Dodoo-Ahrin, K. I. Ozoemena, and N. Manyala, J. Mater. Sci. **40**, 6707 (2013).
[9] D.-W. Wang, F. Li, and H.-M. Cheng, J. Power Sources **185**, 1563 (2008).
[10] C. Zhao, W. Zheng, X. Wang, H. Zhang, X. Cui, and H. Wang, Sci. Rep. **3**, 2986 (2013).
[11] G. Chen, S. S. Liaw, B. Li, Y. Xu, M. Dunwell, S. Deng, H. Fan, and H. Luo, J. Power Sources **251**, 338 (2014).
[12] H. Wang, H. S. Casalongue, Y. Liang, and H. Dai, J. Am. Chem. Soc. **132**, 7472 (2010).
[13] H. B. Li, M. H. Yu, F. X. Wang, P. Liu, Y. Liang, J. Xiao, C. X. Wang, Y. X. Tong, and G. W. Yang, Nat. Commun. **4**, 1894 (2013).
[14] J. Wang, Y. Song, Z. Li, Q. Liu, J. Zhou, X. Jing, M. Zhang, and Z. Jiang, Energy & Fuels **24**, 6463 (2010).
[15] L. Wang, D. Wang, X. Y. Dong, Z. J. Zhang, X. F. Pei, X. J. Chen, B. Chen, and J. Jin, Chem. Commun. (Camb). **47**, 3556 (2011).
[16] X. Dong, L. Wang, D. Wang, C. Li, and J. Jin, Langmuir **28**, 293 (2012).
[17] W. Yang, Z. Gao, J. Wang, J. Ma, M. Zhang, and L. Liu, ACS Appl. Mater. Interfaces **5**, 5443 (2013).
[18] S. Huang, G.-N. Zhu, C. Zhang, W. W. Tjiu, Y.-Y. Xia, and T. Liu, ACS Appl. Mater. Interfaces **4**, 2242 (2012).
[19] Z. Gao, J. Wang, Z. Li, W. Yang, and B. Wang, Chem. Mater. **23**, 3509 (2011).
[20] Z. Lu, W. Zhu, X. Lei, G. R. Williams, D. O'Hare, Z. Chang, X. Sun, and X. Duan, Nanoscale **4**, 3640 (2012).
[21] L. Zhang, X. Zhang, L. Shen, B. Gao, L. Hao, X. Lu, F. Zhang, B. Ding, and C. Yuan, J. Power Sources **199**, 395 (2012).
[22] J. Yang, C. Yu, X. Fan, Z. Ling, J. Qiu, and Y. Gogotsi, J. Mater. Chem. A **1**, 1963 (2013).
[23] Q. Wang and D. O'Hare, Chem. Rev. **112**, 4124 (2012).
[24] X.-M. Liu, Y.-H. Zhang, X.-G. Zhang, and S.-Y. Fu, Electrochim. Acta **49**, 3137 (2004).
[25] M. T. Pettes, H. Ji, R. S. Ruoff, and L. Shi, Nano Lett. **12**, 2959 (2012).
[26] S. Khamlich, A. Bello, M. Fabiane, B. D. Ngom, and N. Manyala, J. Solid State Electrochem. **17**, 2879 (2013).
[27] X.-C. Dong, H. Xu, X.-W. Wang, Y.-X. Huang, M. B. Chan-Park, H. Zhang, L.-H. Wang, W. Huang, and P. Chen, ACS Nano **6**, 3206 (2012).
[28] U. M. Patil, J. S. Sohn, S. B. Kulkarni, S. C. Lee, H. G. Park, K. V. Gurav, J. H. Kim, and S. C. Jun, ACS Appl. Mater. Interfaces **6**, 2450 (2014).
[29] Y. Song, J. Wang, Z. Li, D. Guan, T. Mann, Q. Liu, M. Zhang, and L. Liu, Microporous Mesoporous Mater. **148**, 159 (2012).
[30] Y. Tao, L. Ruiyi, L. Zaijun, L. Junkang, W. Guangli, and G. Zhiquo, RSC Adv. **3**, 19416 (2013).
[31] G. Hu and D. O'Hare, J. Am. Chem. Soc. **127**, 17808 (2005).
[32] C. Burda, X. Chen, R. Narayanan, and M. A. El-Sayed, Chem. Rev. **105**, 1025 (2005).
[33] L.-S. Zhong, J.-S. Hu, H.-P. Liang, A.-M. Cao, W.-G. Song, and L.-J. Wan, Adv. Mater. **18**, 2426 (2006).
[34] L. Xu, Y. Ding, C. Chen, L. Zhao, C. Rimkus, R. Joesten, and S. L. Suib, 308 (2008).
[35] S. J. Chae, F. Güneş, K. K. Kim, E. S. Kim, G. H. Han, S. M. Kim, H.-J. Shin, S.-M. Yoon, J.-Y. Choi, M. H. Park, C. W. Yang, D. Pribat, and Y. H. Lee, Adv. Mater. **21**, 2328 (2009).
[36] W. L. Bragg, in *Proc. Camb. Philol. Soc.* (1913), pp. 43–57.
[37] G. Brindley and S. Kikkawa, Thermochim. Acta **2**, 385 (1978).
[38] J. Olanrewaju, B. Newalkar, C. Mancino, and S. Komarneni, Mater. Lett. 307 (2000).
[39] E. Kanezaki, K. Kinugawa, and Y. Ishikawa, Chem. Phys. Lett. **226**, 325 (1994).
[40] S. Velu, V. Ramkumar, A. Narayanan, and C. Swamy, J. Mater. Sci. **32**, 957 (1997).
[41] A. Bello, O. O. Fashedemi, M. Fabiane, J. N. Lekitima, K. I. Ozoemena, and N. Manyala, Electrochim. Acta **114**, 48 (2013).
[42] L. Zhang, J. Wang, J. Zhu, X. Zhang, K. San Hui, and K. N. Hui, J. Mater. Chem. A **1**, 9046 (2013).
[43] H. Saikia, N. Sarmah, and J. N. Ganguli, Bull. Catal. Soc. India **11**, 1 (2012).
[44] B. Wang, Q. Liu, Z. Qian, X. Zhang, J. Wang, Z. Li, H. Yan, Z. Gao, F. Zhao, and L. Liu, J. Power Sources **246**, 747 (2014).
[45] G. Wang, J. Yang, J. Park, X. Gou, B. Wang, H. Liu, and J. Yao, J. Phys. Chem. C **112**, 8192 (2008).
[46] A. C. Ferrari and J. Robertson, Phys. Rev. B **61**, 14095 (2000).
[47] J. Yu, J. C. Yu, W. Ho, M. K.-P. Leung, B. Cheng, G. Zhang, and X. Zhao, Appl. Catal. A Gen. **255**, 309 (2003).
[48] Z. Wang, X. Zhang, J. Wang, L. Zou, Z. Liu, and Z. Hao, J. Colloid Interface Sci. **396**, 251 (2013).
[49] M. Zhi, C. Xiang, J. Li, M. Li, and N. Wu, Nanoscale **5**, 72 (2013).
[50] H. KuanXin, Z. Xiaogang, and L. Juan, Electrochim. Acta **51**, 1289 (2006).
[51] V. Khomenko, E. Frackowiak, and F. Béguin, Electrochim. Acta **50**, 2499 (2005).
[52] Z. J. Lao, K. Konstantinov, Y. Tournaire, S. H. Ng, G. X. Wang, and H. K. Liu, J. Power Sources **162**, 1451 (2006).